

©2019 IEEE. Personal use of this material is permitted. Permission from IEEE must be obtained for all other uses, in any current or future media, including reprinting/republishing this material for advertising or promotional purposes, creating new collective works, for resale or redistribution to servers or lists, or reuse of any copyrighted component of this work in other works.

arXiv:1902.11046v1 [cs.LG] 28 Feb 2019

GCNv2: Efficient Correspondence Prediction for Real-Time SLAM

Jiexiong Tang¹, Ludvig Ericson¹, John Folkesson¹ and Patric Jensfelt¹

Abstract—In this paper, we present a deep learning-based network, GCNv2, for generation of keypoints and descriptors. GCNv2 is built on our previous method, GCN, a network trained for 3D projective geometry. GCNv2 is designed with a binary descriptor vector as the ORB feature so that it can easily replace ORB in systems such as ORB-SLAM. GCNv2 significantly improves the computational efficiency over GCN that was only able to run on desktop hardware. We show how a modified version of ORB-SLAM using GCNv2 features runs on a Jetson TX2, an embedded low-power platform. Experimental results show that GCNv2 retains almost the same accuracy as GCN and that it is robust enough to use for control of a flying drone.

I. INTRODUCTION

The ability estimate position is key to most, if not all, robotics application involving mobility. In this paper we focus on the problem of visual odometry (VO), i.e. relative motion estimation based on visual information. This is the corner stone in vision-based SLAM systems, which will be the setting we will demonstrate our work in. As in our previous work, [1], we estimate the motion using only an RGB-D sensor, and our target platform is a drone operating in an indoor environment. The RGB-D sensor makes scale directly observable without the need for visual-inertial integration or the computational cost of inferring depth using a neural network as in [2], [3], [4]. This increases robustness, which is a key property when used on a drone and in particular for indoor environments where the margin for error is small and there is typically less obvious textures than in outdoor environments. Our method is designed to be applicable to any system simply by adding an RGB-D sensor, without the need for complicated calibration and synchronisation routines with additional sensors, such as cameras or IMUs. Fusion can instead take place at a lower rate and with less need for precise timing, which, for example, makes integration with the flight control system of a drone simpler.

Like many other areas of research, there is a trend in SLAM to investigate deep learning-based methods. In [5] a keypoint detector and descriptor called SuperPoint is presented. Experimental results show that this CNN-based method has more distinctive descriptors than classical descriptors such as SIFT, and a detector on par with them. However, evaluation on homography estimation in [5] shows that it is only working on par with other keypoint extractors, classical or learning-based. In our previous work [1],

This work was partially supported by the Wallenberg AI, Autonomous Systems and Software Program (WASP), the SSF project FACT and the VR grant XPLORE3D.

¹The authors are all with the Centre for Autonomous Systems at KTH Royal Institute of Technology, Stockholm, SE-10044, Sweden jiexiong@kth.se

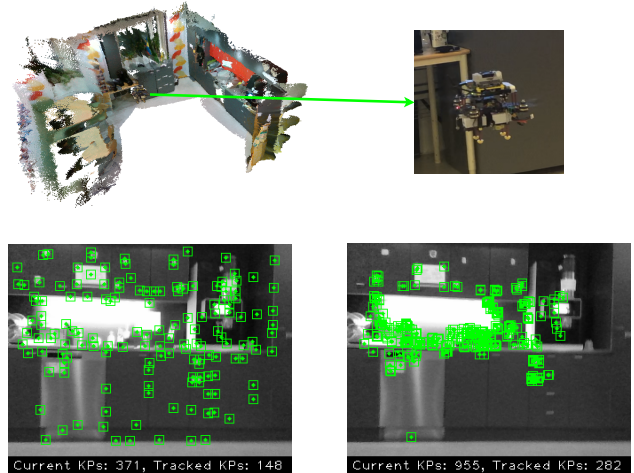


Fig. 1: The top figure shows our drone performing position hold using GCN-SLAM. The figures below show the intermediate output for comparison of binary features, ORB and GCNv2, in ORB-SLAM2 and GCN-SLAM respectively. GCNv2 (left) tends to predict more repeatable and evenly distributed features compared with ORB (right.)

presented before SuperPoint, we introduced the Geometric Correspondence Network, GCN, specifically tailored for producing keypoints for camera motion estimation, achieving better accuracy than classical methods. However, due to the computation and structure limitation of GCN, it is difficult to achieve real-time performance in a fully-operational system, e.g. on board a drone. Both keypoint extraction and matching are computationally too expensive. Furthermore, due to the multi-frame matching setup, integrating GCN into existing SLAM systems becomes non-trivial.

In this paper we introduce GCNv2, based on the conclusions from [1], to improve computational efficiency while still maintaining the high precision of GCN. Our contributions are:

- GCNv2 maintains the accuracy of GCN, providing significant improvements in motion estimation in comparison to related deep learning-based feature extraction methods as well as classical methods.
- The inference of GCNv2 can run on embedded low-power hardware, such as a Jetson TX2, compared to GCN which requires a desktop GPU for real-time inference.
- We design GCNv2 to have the same descriptor format as the ORB feature so that it can be drop-in substituted as the keypoint extractor in SLAM systems like ORB-

SLAM2 [6] or SVO2 [7].

- We demonstrate the effectiveness and robustness of our work by using GCN-SLAM¹ on a real drone for control, and show that it handles situations where ORB-SLAM2 fails.

II. RELATED WORK

In this section we cover related work in two areas. First VO and SLAM methods are covered and then we focus specifically on work on deep learning-based methods for image correspondence.

A. VO and SLAM

In direct methods for VO and SLAM, motion is estimated by aligning frames based directly on the pixel intensities, with [8] being an early example. DVO (Direct Visual Odometry), presented in [9], adds a pose graph to reduce the error. DSO [10] is a direct and sparse method that adds joint optimisation of all model parameters. An alternative to the frame-to-frame matching is to match each new frame to a volumetric representation as in KinectFusion [11], Kintinous [12] and ElasticFusion [13].

In indirect methods, the first step in a typical pipeline is to extract keypoints, which are then matched to previous frames to estimate the motion. The matching is based on the keypoint descriptors and geometric constraints. The state-of-the-art in this category is still defined by ORB-SLAM2 [14], [6]. The ORB descriptor is a binary vector allowing high-performance matching.

Somewhere between direct and indirect methods we find the semi-direct approaches. SVO2 [7] is a sparse method in this category, and can run at hundreds of Hertz. There are also semi-dense methods, in which category LSD-SLAM [15] was one of the first. RGBDTAM [16] combines both semi-dense photometric and dense geometric errors for pose estimation.

There are a number of recent deep learning-based mapping systems like [17], [18]. The focus in these methods is deep learning-based single view depth estimation to reduce the scale drift inherent in monocular systems. CNN-SLAM [17] feeds the depth into LSD-SLAM. In DVSO [19], depth is predicted in a similar way to [2], using a virtual stereo view. CodeSLAM [20] learns an optimizable representation from conditioned auto-encoding for 3D reconstruction. In S2D [21], we build on DSO [10] and exploit both depth and normals predicted by a jointly optimised CNN. Some work on end-to-end training for motion estimation also exist. Image reconstruction loss is used for unsupervised learning in [4], [22]. However, geometry-based optimization methods still outperform end-to-end systems as shown in [19].

B. Deep Correspondence Matching

There is an abundance of recent works that deploy variants of metric learning for training deep features for finding image correspondences [23], [24], [25], [26], [27], [28], [29], [30], [5]. Works in [31], [32] focus on improving

learning-based detection with better invariances. Aimed at a different aspect, [33], [34], [35] use synthetic samples generated in a self-supervised manner to improve general feature matching.

Among the aforementioned methods, LIFT [29] in particular uses a patch-based method to perform both keypoint detection and descriptor extraction. SuperPoint [5] predicts the keypoints and descriptors using a single network together with the self-supervised strategy in [35]. Notably, [5] shows that [5], [29], [30] work on par with classical methods like SIFT for motion estimation.

In GCN [1], we show that by learning keypoints and descriptors specifically targeting motion estimation, performance is improved – contrary to what is reported for other more general deep learning-based keypoint extractor systems [5], [30]. In this paper we introduce an extension to GCN, GCNv2. We demonstrate the applicability of these keypoints for SLAM and build on ORB-SLAM2 as it offers a comprehensive multi-threaded state-of-the-art indirect SLAM system with support for monocular as well as RGB-D cameras. ORB-SLAM2 complements the tracking front-end with a back-end that does both pose graph optimisation using g2o [36] and loop closure detection using a binary bag of words representation [37]. To simplify this integration, we design the GCNv2 descriptor to have the same format as that of ORB.

III. GEOMETRIC CORRESPONDENCE NETWORK

In this section, we present the design of GCNv2, aimed at making it suitable for real-time SLAM applications running on embedded hardware rather than a powerful desktop computer. We first introduce the modifications to the network structure. Then, we present the training scheme for the binarized feature descriptor and keypoint detector.

A. Network Structure

The original GCN structure, proposed in [1], consists of two major parts: an FCN [38] structure with a ResNet-50 backbone and a bidirectional convolutional network. The FCN is adopted for dense feature extraction and the bidirectional network is used for temporal keypoint prediction. Although impressive tracking performance has been achieved using GCN compared with existing methods, GCN has practical limitations when it comes to the use in a real-time SLAM system with limited hardware. The network architecture requires relatively powerful computational hardware which renders it unable to run in real-time on board e.g. the Jetson TX2 used on our drone. Furthermore, the bidirectional structure requires matching between two or more frames at the same time. This significantly increases computational complexity for a window-based SLAM method, since keyframes then are updated dynamically based on the current camera position.

Inspired by SuperPoint [5], which uses a simple structure to perform detection using a single frame, we deploy a network with even fewer parameters and working on a lower scale than SuperPoint. Intuitively, the network performs an

¹Built on ORB-SLAM2 with ORB substituted for GCNv2

individual prediction for each grid cell of size 16×16 pixels in the original image. In GCNv2 all the pooling layers are replaced by convolutions with kernel size 4×4 , stride 2 and padding 1. As in SuperPoint, the network takes 320×240 images as input. This is also the image size we used later for SLAM. Further details on the GCNv2 network specifics can be found in our publicly available source code².

GCN-SLAM with GCNv2 runs at 20 Hz on Jetson TX2 and runs at around 80 Hz on a laptop with Intel i7-7700HQ and mobile version NVIDIA 1070. To achieve even higher frame rates we introduce a smaller version of GCNv2, called GCNv2-tiny, where we reduce the number of feature maps by half from the second layer and onward. GCN-SLAM with GCNv2-tiny runs at 40 Hz on a TX2 and is therefore well-suited for deployment on a drone.

B. Feature Extractor

Binarized Descriptor We trained the features of GCNv2 to be binary for accelerating the matching procedure and to match those of ORB. To binarize the features, we add a binary activation layer on top the final output. It is essentially a hard sign function and is therefore not differentiable. The challenge is how to back-propagate the loss properly through this layer of the network. We used the method proposed in [39]. The binary activation layer can be written as follows:

$$\begin{aligned} \text{Forward: } \mathbf{b}(\mathbf{x}) &= \text{sign}(\mathbf{f}(\mathbf{x})) = \begin{cases} +1 & \mathbf{f}(\mathbf{x}) \geq 0 \\ -1 & \text{otherwise} \end{cases} \\ \text{Backward: } \frac{\partial \mathbf{b}}{\partial \mathbf{f}} &= \frac{\partial L_{metric}}{\partial \mathbf{b}} \mathbf{1}_{|\mathbf{f}| \leq 1} \end{aligned} \quad (1)$$

where $\mathbf{x} = (u, v)$ is the 2D coordinates in the image and $\mathbf{f}(\cdot)$ is the feature vector at a given location. L_{metric} is the loss for metric learning. $\mathbf{1}$ is the indicator function. We found that it is more efficient to train the network with the above method rather than forcing the network to directly predict a binary output by minimizing quantification loss as in [40]. One possible reason is that forcing the value to be clustered around $\{+1, -1\}$ conflicts with the metric learning that follows, which uses distance as margin making the training unstable.

The number of feature maps \mathbf{f} is set to 256 to make the descriptor have the same bit width as ORB features so that the descriptor can be directly incorporated into existing ORB-based visual tracking systems.

Nested Metric Learning The pixel-wise metric learning is used for training the descriptor in a nearest-neighbour manner. The triplet loss for binarized features is as follows:

$$\begin{aligned} L_{metric} &= \sum_i \max(0, d_{\mathbf{x}_i, \mathbf{x}_{i,+}} - d_{\mathbf{x}_i, \mathbf{x}_{i,-}} + m) \\ d_{\mathbf{x}_1, \mathbf{x}_2} &= (\text{sign}(\mathbf{f}_1(\mathbf{x}_1)) - \text{sign}(\mathbf{f}_2(\mathbf{x}_2)))^2 \end{aligned} \quad (2)$$

where m is the distance margin for the truncation. d is equivalent to the squared Hamming distance for the 32-byte descriptor. We use the squared distance since we found it leads to faster and better convergence for training. $(\mathbf{x}_i, \mathbf{x}_{i,+})$

Algorithm 1: Exhaustive Negative Sample Mining

Input : Feature in 1st frame: $\mathbf{f}_1(\mathbf{x}_i)$,
Features in 2nd frame: $\{\mathbf{f}_2(\mathbf{x}_j) \mid j \in [0, N]\}$,
Correspondence Ground Truth: $\mathbf{x}_{i,+}$,
Relaxed Criteria: $\mathbf{c} = (u_c, v_c)$
Output: Negative sample $\mathbf{f}_2(\mathbf{x}_{i,-})$ **or** None
1 k-NN Matching: Find top k matched \mathbf{x}_j using Hamming distance
2 for $n = 1; n \leq k; n++$ **do**
3 Query the n th nearest distance \mathbf{x}_j^n
4 **if** $\text{abs}(\mathbf{x}_j^n - \mathbf{x}_i) < \mathbf{c}$ **then**
5 **return** $\mathbf{f}_2(\mathbf{x}_j^n)$
6 **end**
7 end
8 return None

is a matching pair obtained using the ground truth camera poses from the training data as follows:

$$\mathbf{x}_{i,+} = \pi^{-1}(\mathbf{R}_{gt} \cdot \pi(\mathbf{x}_i, d_i) + \mathbf{t}_{gt}) \quad (3)$$

where $\mathbf{R} \in \mathbb{R}^{3 \times 3}$ is the rotation matrix and $\mathbf{t} \in \mathbb{R}^3$ is the translation vector. $(\mathbf{x}_i, \mathbf{x}_{i,-})$ is a non-matching pair retrieved by negative sample mining. The mining procedure is described in algorithm 1. The exhaustive search will further penalize the already matched features with the relaxed criteria described in [1]. The relaxed criteria is used to increase the tolerance to potentially noisy data.

C. Distributed Keypoint Detector

The training loss for keypoint detection is the same as in the original GCN. It is computed using two consecutive frames as follows:

$$\begin{aligned} L_{mask} &= L_{ce}(\mathbf{o}_1, \mathbf{x}) + L_{ce}(\mathbf{o}_2, \mathbf{x}_+) \\ L_{ce}(\mathbf{o}, \mathbf{x}) &= -\sum_i (\alpha_1 c_{\mathbf{x}_i} \log(\mathbf{o}(\mathbf{x}_i)) + \alpha_2 (1 - c_{\mathbf{x}_i}) \log(1 - \mathbf{o}(\mathbf{x}_i))) \end{aligned} \quad (4)$$

A notable difference from SuperPoint is that GCNv2 specifically targets motion estimation. SuperPoint tries to accomplish SIFT-like corner detection and its performance gain can chiefly be attributed to its superior descriptor. However, a CNN is capable of generating more representative features with a larger receptive field than classical methods. We therefore generate the ground truth by detecting Shi-Tomasi corners in a 16×16 grid and warp them to the next frame using eq. (3). This leads to better distribution of keypoints and the objective function directly reflects the ability to track the keypoints based on texture.

D. Training Details

The triplet loss in eq. (2) and cross entropy in eq. (4) are weighted by 100, 1 during training to provide a coarse normalization of the two terms. The learning rate for the adaptive gradient descent method, ADAM [41], used for training is started from 10^{-4} and halved every 40 epoch for a total of 100 training epochs. The weights of GCNv2 are randomly initialized. We mapped the squared Hamming

²https://github.com/jiexiong2016/GCNv2_SLAM

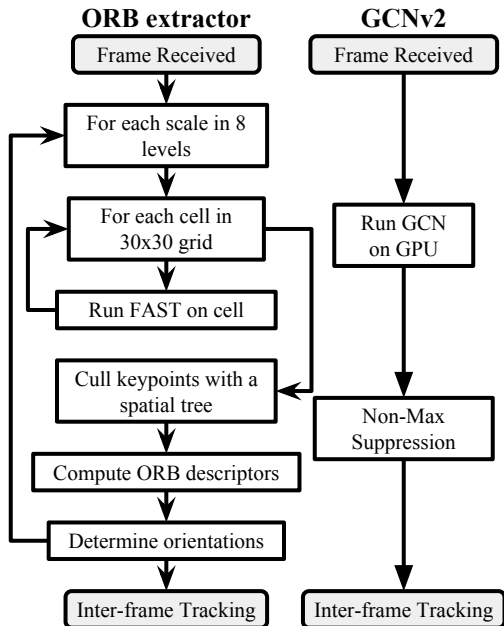


Fig. 2: Illustration of the original ORB-SLAM2 keypoint extraction process on the left side, and our method on the right. The keypoint extraction in GCN-SLAM is comparatively simple, in large part because it relies on 2D convolutions and matrix multiplication which is off-loaded to the GPU.

distance to the L_2 unit sphere to perform the fast nearest neighbour matching as in [5]. The margin for the triplet loss is set to 1. The weights $[\alpha_1, \alpha_2]$ of the weighted cross entropy is set to $[0.1, 1.0]$.

IV. GCN-SLAM

One of the most important design choices for a keypoint-based SLAM system is the choice of keypoint extractor. The keypoints are often re-used at multiple stages in such systems. ORB features [42], the namesake of ORB-SLAM2, are a particularly well-suited candidate as ORBs are invariant to rotation and scale, cheap to compute compared to other keypoint detectors with equivalent properties such as SIFT or SURF, and have a binary feature vector to cater for fast matching.

As previously shown [1], GCN used in a naive motion estimation pipeline performs better than or on par with ORB-SLAM2 [6]. Notably, this is without higher-order SLAM functionality such as pose graph optimization, global bundle adjustment, or loop detection. Incorporating GCN into a system with such functionality would therefore be likely to yield better results. However, as mentioned, GCN is prohibitively expensive for real-time use on embedded hardware which we target in this work. In what follows we show how we modify ORB-SLAM2 to incorporate GCNv2, in a system we call GCN-SLAM.

ORB-SLAM2’s motion estimation is based on frame-to-frame keypoint tracking and feature-based bundle adjustment. We will briefly describe the detection and description of these features. ORB-SLAM2 employs a *scale pyramid*

where the input image is iteratively scaled down to enable multi-scale feature detection by running single-scale algorithms on the multiple rescaled images. For each scale level, the FAST corner detector is applied in a 30×30 grid. If no detections are found in a cell, FAST is run again with a decreased threshold. After all detections have been gathered from all cells at a given level in the scale pyramid, a space partitioning algorithm is used to cull the keypoints first by their image coordinates, then by detection score. Finally, once typically 1000 keypoints have been selected in total, the viewing angle of each keypoint is computed, then each pyramid scale level is filtered with Gaussian blur, and the 256-bit ORB descriptor for each keypoint at each level is computed from the blurred image.

Our method computes both keypoint locations and descriptors simultaneously in a single forward-pass of the network, and as stated before, its end result is designed to be a drop-in replacement for the ORB feature extractor outlined above. In GCNv2, we input a single grey image frame to the network which outputs two matrices: a $1 \times 320 \times 240$ keypoint mask, and a $256 \times 320 \times 240$ feature descriptor matrix. The keypoint mask is thresholded to obtain a set of keypoint locations, their confidences, and their corresponding 256-bit feature descriptors. As in [5], we apply non-maximum suppression with a grid size of 8×8 . As it is not possible to know the orientation of the detected features, we set the angle to zero. The two keypoint methods are illustrated in fig. 2.

Once keypoints and their respective descriptors are found, ORB-SLAM2 relies primarily on two methods for frame-to-frame tracking: first, by assuming constant velocity and projecting the previous frame’s keypoints into the current frame, and if that fails, by matching the keypoints of the current frame to the last-created keyframe using bag-of-words similarity. We have disabled the former so as to use only use the latter keypoint-based reference frame tracking. We have also replaced the matching algorithm with a standard nearest-neighbor search in our experiments. These modifications are made to examine the performance of our keypoint extraction method, rather than that of ORB-SLAM2’s other tracking heuristics.

Finally, we have left ORB-SLAM2’s loop closure and pose graph optimization intact, apart from having regenerated the bag-of-words vocabulary to suit GCNv2 feature descriptors by computing them on the training dataset presented in section V-A.

V. EXPERIMENTAL RESULTS

In this section, we present experimental results to justify our conclusions regarding the performance of our keypoint extraction method, and its embodiment in the GCN-SLAM system. We first introduce our training dataset, then four datasets on which we examined our method’s performance and compare to some related methods, and finally we outline the quantitative and qualitative conclusions of these results.

Note that our aim in this section is not to show that GCN-SLAM is better than ORB-SLAM2 but to show that GCNv2 is: i) better suited for accurate motion estimation, ii)

TABLE I: ATE USING FRAME TO FRAME TRACKING

Dataset (200 Frames)	GCN	ORB	SIFT	SURF	SuperPoint	GCNv2	GCNv2-tiny	GCNv2-large
fr1_floor	0.015m	0.080m	0.073m	0.074m	-	-	-	-
fr1_desk	0.037m	0.151m	0.144m	0.148m	0.166m	0.049m	0.084m	0.038m
fr1_360	0.059m	0.278m	0.305m	0.279m	-	-	-	0.097m
fr3_long_office	0.061m	0.090m	0.076m	0.070m	0.105m	0.046m	0.085m	0.067m
fr3_large_cabinet	0.073m	0.097m	0.091m	0.143m	0.195m	0.064m	0.067m	0.056m
fr3_nst	0.020m	0.061m	0.036m	0.030m	0.055m	0.018m	0.024m	0.021m
fr3_nnf	0.221m	-	-	-	-	-	-	-

computationally efficient, and iii) providing robustness for a SLAM system.

In the results below, evaluations on datasets were performed on a laptop with an Intel i7-7700HQ and a mobile version of NVIDIA 1070. For real-world experiments we used an NVIDIA Jetson TX2 embedded computer for processing and an Intel RealSense D435 RGB-D camera sensor on our drone (see fig. 1.)

A. Training Data

The original GCN was trained using the TUM dataset from sensor fr2. It provides accurate pose through a motion capturing system. In GCNv2, we trained the network using a subset of the SUN-3D [43] dataset we created in our recent work [21]. SUN-3D contains millions of real-world recorded RGB-D images in various typical indoor environments. A total 44,624 frames were extracted by roughly one frame per second from the videos. It is very large and can potentially produce a more generalized network. However, the ground truth poses provided by SUN-3D are estimated by visual tracking with loop closure and so are relatively accurate globally, but have misalignments at frame level. To account for this local error, we extract SIFT features and use the provided poses as initial guesses for bundle adjustment to update the relative pose of each frame pair. In this sense, the training of GCNv2 is using self-annotated data with only vision information.

B. Quantitative Results

For comparison with the original GCN, we select the same sequences of the TUM datasets as in [1] and evaluating tracking performance with an open and a closed loop system. We use the Absolute trajectory error (ATE) as the metric.

Since we trained GCNv2 on a different dataset than the original GCN [1], we also show results using the original recurrent structure for comparison. We have therefore also created GCNv2-large, with ResNet-18 as the backbone and deconvolutional up-sampling for the feature maps. The bi-directional feature detector is moved to the lowest scale as the other two versions of GCNv2.

Frame-to-frame tracking results are shown in table I. The first columns, before SuperPoint, are from [1] where 640x480 images were used and GCN was trained on TUM fr2 data only. All versions of GCNv2 use the same image resolution as SuperPoint, i.e. 320x240. The results are consistent with the results reported in [5], SuperPoint performs on par with classical method like SIFT. GCNv2 has a performance close

TABLE II: ATE USING CLOSED LOOP SYSTEM

Dataset	GCN	ORB SLAM2	Elastic Fusion	RGBD TAM	GCN SLAM
fr1_floor	0.038m	0.036m	-	-	0.021m
fr1_desk	0.029m	0.016m	0.020m	0.027m	0.031m
fr1_360	0.069m	0.213m	0.108m	0.101m	0.155m
fr3_long_office	0.040m	0.010m	0.017m	0.027m	0.021m
fr3_large_cabinet	0.097m	-	0.099m	0.070m	0.070m
fr3_nst	0.020m	0.019m	0.016m	0.010m	0.014m
fr3_nnf	0.064m	-	-	-	0.086m

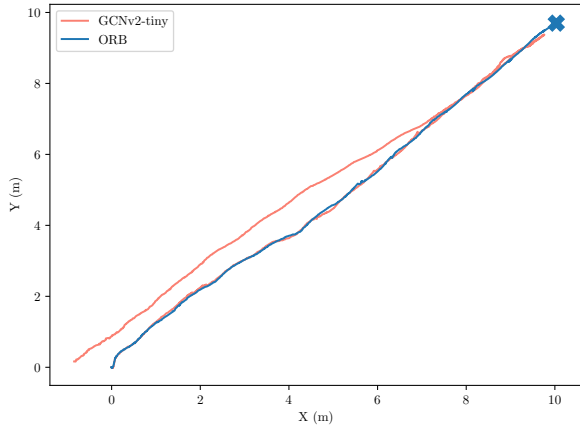
to GCN, and like GCN, significantly better than both SuperPoint and classical keypoints. GCNv2 performance is on par with GCN, and even slightly better in two cases – likely due to using a much larger dataset for training. The exceptions are fr1_floor and fr1_360. These sequences require fine details, and the detection and descriptor extraction in GCNv2 is performed with a lower scale feature map for efficiency, though GCNv2-large handles one of these sequences. The smaller version of GCNv2, GCNv2-tiny, is only slightly less accurate than GCNv2.

In table II, we compare the closed loop performance of GCN-SLAM with our previous work, as well as ORB-SLAM2, Elastic Fusion, and RGBDTAM. GCN-SLAM successfully tracks the position in all sequences with an error similar to that of GCN, whereas ORB-SLAM2 fails on two sequences. GCNv2 has significantly reduced drift error compared to ORB-SLAM2 in the fast rotations of fr1_360. It is also noteworthy that for this particular sequence, the original GCN does significantly better than both ORB-SLAM2 and GCN-SLAM. ORB-SLAM2 is tracking well in all other sequences, and the errors of both GCN-SLAM and ORB-SLAM2 are small.

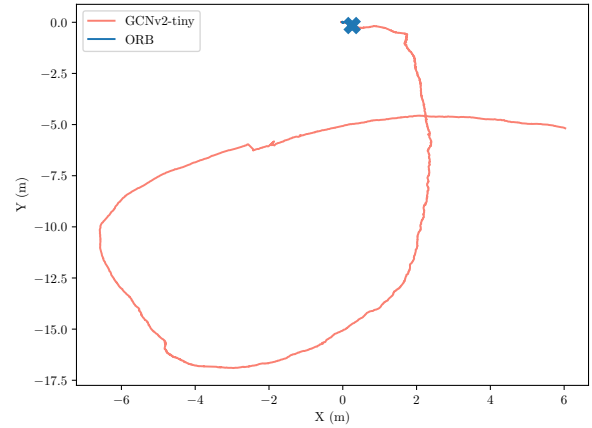
C. Qualitative Results

To further verify the robustness of using GCNv2 in a real-world SLAM system, we show results on datasets collected in our environment under different conditions: a) going up a corridor, turning 180 degrees and walking back with a handheld camera, b) walking in a circle on an outdoor parking lot with a handheld sensor in daylight, c) flying in an alcove with windows and turning 180 degrees, and d) flying in a kitchen and turning 360 degrees while using GCN-SLAM for positioning.

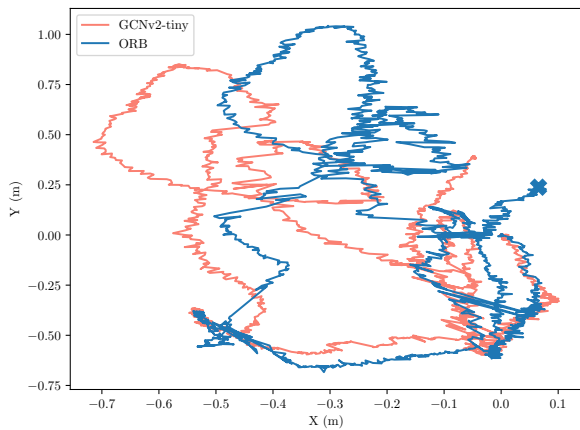
Since they are without ground truth, the results are only qualitative. These datasets were chosen to show that our method handles difficult scenarios, is robust, and can be used for positioning of a real drone. Figure 3 shows the estimated



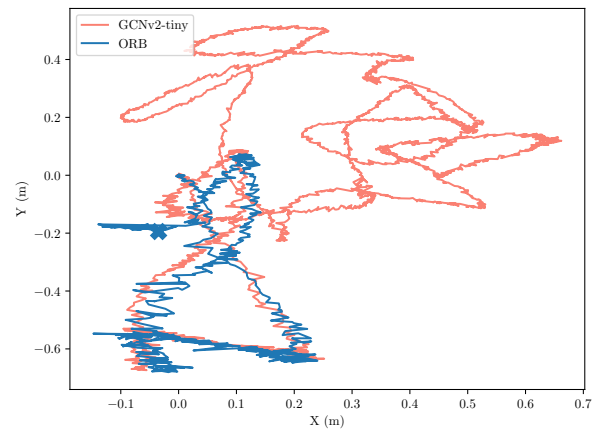
(a) *Corridor*: indoor, handheld.



(b) *Parking lot*: outdoor, handheld.



(c) *Alcove*: indoor, flying with primitive optical flow sensor.



(d) *Kitchen*: indoor, flying with GCN-SLAM for positioning.

Fig. 3: Estimated trajectory on each of the four datasets using the GCN-SLAM pipeline and illustrating the difference between GCNv2 and ORB features. Note that these trajectories do not have any ground truth but we mark track lost with a cross and we see that this happened in all four cases when using ORB features.

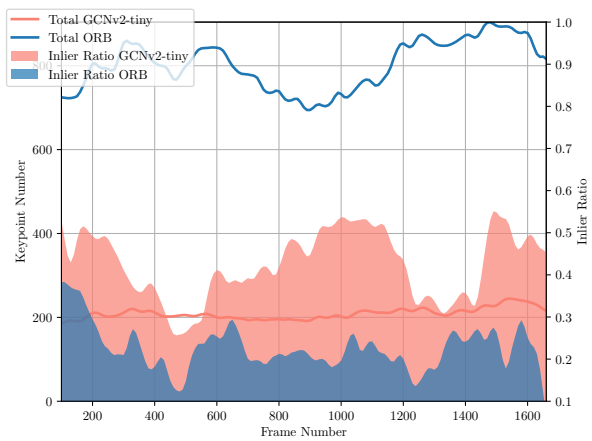
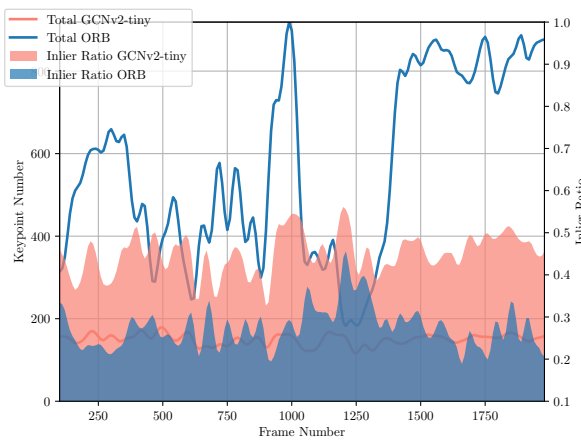
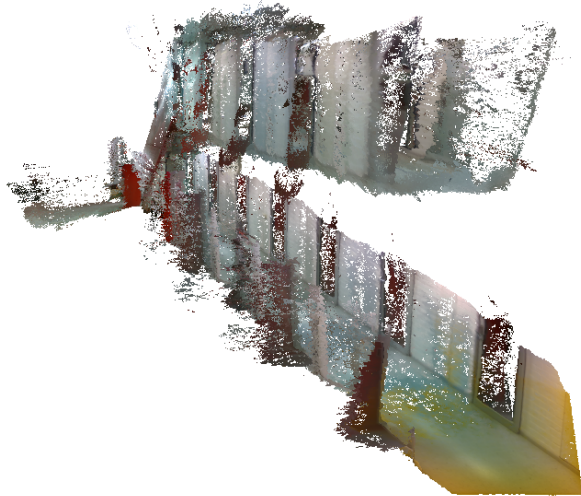


Fig. 4: Keypoint extractor performance in terms of tracking shown for the *Corridor* (left) and *Kitchen* datasets (right.) Lines indicate the total number of keypoints detected per frame. The filled-in area under the lines shows the fraction of keypoints that were successfully used for local map tracking, i.e. contribute to tracking and is plotted against the right-hand axis.



(a) *Lab room: handheld.*



(b) *Lab corridor: handheld.*

Fig. 5: Mesh reconstruction results using GCN-SLAM as input to TSDF volume integration from Open3D. Loop closure detection in GCN-SLAM was disabled to demonstrate the accuracy in the tracking alone.

trajectory of GCN-SLAM using ORB versus GCNv2 as keypoints. Note that both features are evaluated in exactly the same tracking pipeline for fair comparison, i.e. GCNv2 or ORB features is the *only* differences. Refer to the source-code for further details. using GCN-SLAM as a basis for drone control improves performance as can be seen by comparing figs. 3c and 3d. In fig. 3c, the position is estimated using only an optical flow sensor whereas fig. 3d uses GCN-SLAM as a source of position, and it is clear that the drone is able to hold its position better as there is significantly less jitter in this trajectory. In all four datasets, tracking is maintained with GCNv2, but lost with ORB. We used a remote control to send setpoints to the flight control unit on the drone for control, using the built-in position holding mode.

In fig. 4 we compare the performance of our keypoint extractor to the original ORB keypoint extractor. We plot the number of inliers during tracking of the local map for our adapted SLAM system, first with ORB keypoints, and then with GCNv2 keypoints. As the figure illustrates, while there are many more ORB features, our method has a higher percentage of inliers. In addition, as shown in fig. 1, GCNv2 results in better distributed features compared with ORB.

Figure 5 shows the mesh reconstruction using GCN-SLAM output poses from two additional sequences. The left sequence was from an office and the right was acquired walking between two floors using stairs. TSDF volume integration from Open3D³ was used to create the mesh. To show the accuracy of our method, the loop closure detection of GCN-SLAM is disabled.

VI. CONCLUSIONS

In our previous work [1], we showed that our method, GCN, achieves better performance in visual tracking compared with existing deep learning and classical methods. However, it cannot be directly deployed into a real-time SLAM system in an efficient way due to its deep recurrent structure. In this paper, we addressed these issues by proposing a smaller, more efficient version of GCN, called GCNv2, that is readily adaptable to existing SLAM systems. We showed that GCNv2 can be effectively used in a modern feature-based SLAM system to achieve state-of-the-art tracking performance. The robustness and performance of the method was verified by incorporating GCNv2 into GCN-SLAM and using it on-board for positioning on our drone.

Limitations GCNv2 is trained mainly for projective geometry and not generic feature matching. As always with learning-based methods generalization is an important factor. GCNv2 works relatively well for outdoor scenes, as demonstrated in the experiments (Cf. fig. 3b). However, since no outdoor data was used for training, further improvements can likely be made. Our target here is an indoor setting and we did not investigate this further.

Future work In this paper, we mainly improved the efficiency of GCN and achieve stable tracking perform on our platform, a drone with NVIDIA Jetson TX2. However, since the original recurrent structure is removed, there is trade-off between the accuracy and running speed. In the future, we would like to further investigate to use the self-supervised learning to improve our system.

REFERENCES

- [1] J. Tang, J. Folkesson, and P. Jensfelt, “Geometric correspondence network for camera motion estimation,” *IEEE Robotics and Automation*

³<http://www.open3d.org>

- Letters*, vol. 2, no. 2, pp. 1010–1017, 2018.
- [2] C. Godard, O. Mac Aodha, and G. J. Brostow, “Unsupervised monocular depth estimation with left-right consistency,” in *IEEE Conf. on Computer Vision and Pattern Recognition (CVPR)*, vol. 2, 2017.
 - [3] Y. Luo, J. Ren, M. Lin, J. Pang, W. Sun, H. Li, and L. Lin, “Single view stereo matching,” in *IEEE Conf. on Computer Vision and Pattern Recognition (CVPR)*, 2018.
 - [4] T. Zhou, M. Brown, N. Snavely, and D. G. Lowe, “Unsupervised learning of depth and ego-motion from video,” in *IEEE Conf. on Computer Vision and Pattern Recognition (CVPR)*, vol. 2, 2017.
 - [5] D. DeTone, T. Malisiewicz, and A. Rabinovich, “Superpoint: Self-supervised interest point detection and description,” in *CVPR Deep Learning for Visual SLAM Workshop*, 2018.
 - [6] R. Mur-Artal and J. D. Tardós, “ORB-SLAM2: an open-source SLAM system for monocular, stereo and RGB-D cameras,” *IEEE Transactions on Robotics*, vol. 33, no. 5, pp. 1255–1262, 2017.
 - [7] C. Forster, Z. Zhang, M. Gassner, M. Werlberger, and D. Scaramuzza, “SVO: Semidirect visual odometry for monocular and multicamera systems,” *IEEE Trans. on Robotics*, vol. 33, no. 2, pp. 249–265, 2017.
 - [8] A. I. Comport, E. Malis, and P. Rives, “Accurate quadrifocal tracking for robust 3d visual odometry,” in *IEEE Intl. Conf. on Robotics and Automation (ICRA)*, 2007.
 - [9] C. Kerl, J. Sturm, and D. Cremers, “Dense visual slam for rgb-d cameras,” in *2013 IEEE/RSJ Intl. Conf. on Intelligent Robots and Systems*, 2013.
 - [10] J. Engel, V. Koltun, and D. Cremers, “Direct sparse odometry,” *IEEE Trans. Pattern Anal. Mach. Intell.*, March 2018.
 - [11] R. A. Newcombe, S. Izadi, O. Hilliges, D. Molyneaux, D. Kim, A. J. Davison, P. Kohi, J. Shotton, S. Hodges, and A. Fitzgibbon, “Kinectfusion: Real-time dense surface mapping and tracking,” in *2011 10th IEEE Intl. Symposium on Mixed and Augmented Reality*, 2011.
 - [12] T. Whelan, M. Kaess, H. Johannsson, M. Fallon, J. J. Leonard, and J. McDonald, “Real-time large-scale dense rgb-d slam with volumetric fusion,” *Intl. Journal of Robotics Research*, vol. 34, no. 4-5, pp. 598–626, 2015.
 - [13] T. Whelan, R. F. Salas-Moreno, B. Glocker, A. J. Davison, and S. Leutenegger, “Elasticfusion: Real-time dense slam and light source estimation,” *Intl. Journal of Robotics Research*, vol. 35, no. 14, pp. 1697–1716, 2016.
 - [14] R. Mur-Artal, J. M. M. Montiel, and J. D. Tardós, “ORB-SLAM: A versatile and accurate monocular slam system,” *IEEE Trans. on Robotics*, vol. 31, no. 5, pp. 1147–1163, 2015.
 - [15] J. Engel, T. Schöps, and D. Cremers, “Lsd-slam: Large-scale direct monocular slam,” in *European Conf. on Computer Vision (ECCV)*, 2014.
 - [16] A. Concha and J. Civera, “RGBDTAM: A cost-effective and accurate RGB-D tracking and mapping system,” *arXiv:1703.00754*, 2017.
 - [17] K. Tateno, F. Tombari, I. Laina, and N. Navab, “Real-time dense monocular slam with learned depth prediction,” in *IEEE Conf. on Computer Vision and Pattern Recognition (CVPR)*, 2017.
 - [18] N. Yang, R. Wang, J. Stückler, and D. Cremers, “Deep virtual stereo odometry: Leveraging deep depth prediction for monocular direct sparse odometry,” *European Conf. on Computer Vision (ECCV)*, 2018.
 - [19] S. Wang, R. Clark, H. Wen, and N. Trigoni, “DeepVO: Towards end-to-end visual odometry with deep recurrent convolutional neural networks,” in *IEEE Intl. Conf. on Robotics and Automation (ICRA)*, IEEE, 2017.
 - [20] M. Bloesch, J. Czarnowski, R. Clark, S. Leutenegger, and A. J. Davison, “CodeSLAM-learning a compact, optimisable representation for dense visual SLAM,” *arXiv preprint arXiv:1804.00874*, 2018.
 - [21] J. Tang, J. Folkesson, and P. Jensfelt, “Sparse2dense: From direct sparse odometry to dense 3-d reconstruction,” *IEEE Robotics and Automation Letters*, vol. 4, no. 2, pp. 530–537, 2019.
 - [22] R. Li, S. Wang, Z. Long, and D. Gu, “UnDeepVO: Monocular visual odometry through unsupervised deep learning,” *arXiv preprint arXiv:1709.06841*, 2017.
 - [23] J. Zbontar, Y. LeCun *et al.*, “Stereo matching by training a convolutional neural network to compare image patches,” *Journal of Machine Learning Research*, vol. 17, no. 1-32, p. 2, 2016.
 - [24] D. Gadot and L. Wolf, “PatchBatch: A batch augmented loss for optical flow,” in *IEEE Conf. on Computer Vision and Pattern Recognition (CVPR)*, 2016, pp. 4236–4245.
 - [25] A. Zeng, S. Song, M. Nießner, M. Fisher, J. Xiao, and T. Funkhouser, “3DMatch: Learning local geometric descriptors from RGB-D reconstructions,” in *IEEE Conf. on Computer Vision and Pattern Recognition (CVPR)*, 2017, pp. 1802–1811.
 - [26] T.-Y. Yang, J.-H. Hsu, Y.-Y. Lin, and Y.-Y. Chuang, “DeepCD: Learning deep complementary descriptors for patch representations,” in *IEEE Intl. Conf. on Computer Vision (ICCV)*, 2017, pp. 3314–3322.
 - [27] X. Zhang, F. X. Yu, S. Kumar, and S.-F. Chang, “Learning spread-out local feature descriptors,” in *IEEE Intl. Conf. on Computer Vision (ICCV)*, 2017, pp. 4595–4603.
 - [28] M. E. Fathy, Q.-H. Tran, M. Zeeshan Zia, P. Vernaza, and M. Chandraker, “Hierarchical metric learning and matching for 2D and 3D geometric correspondences,” in *European Conf. on Computer Vision (ECCV)*, 2018, pp. 803–819.
 - [29] K. M. Yi, E. Trulls, V. Lepetit, and P. Fua, “Lift: Learned invariant feature transform,” in *European Conf. on Computer Vision (ECCV)*, B. Leibe, J. Matas, N. Sebe, and M. Welling, Eds., 2016, pp. 467–483.
 - [30] C. B. Choy, J. Gwak, S. Savarese, and M. Chandraker, “Universal correspondence network,” in *Advances in Neural Information Processing Systems (NIPS)*, 2016.
 - [31] Y. Verdie, K. Yi, P. Fua, and V. Lepetit, “Tilde: A temporally invariant learned detector,” in *IEEE Conf. on Computer Vision and Pattern Recognition (CVPR)*, 2015, pp. 5279–5288.
 - [32] N. Savinov, A. Seki, L. Ladicky, T. Sattler, and M. Pollefeys, “Quadnetworks: unsupervised learning to rank for interest point detection,” in *IEEE Conf. on Computer Vision and Pattern Recognition (CVPR)*, 2017, pp. 1822–1830.
 - [33] S. Honari, P. Molchanov, S. Tyree, P. Vincent, C. Pal, and J. Kautz, “Improving landmark localization with semi-supervised learning,” in *IEEE Conf. on Computer Vision and Pattern Recognition (CVPR)*, 2018, pp. 1546–1555.
 - [34] I. Rocco, R. Arandjelovic, and J. Sivic, “Convolutional neural network architecture for geometric matching,” in *IEEE Conf. on Computer Vision and Pattern Recognition (CVPR)*, 2017, pp. 6148–6157.
 - [35] D. DeTone, T. Malisiewicz, and A. Rabinovich, “Deep image homography estimation,” *arXiv preprint arXiv:1606.03798*, 2016.
 - [36] R. Kimmerle, G. Grisetti, H. Strasdat, K. Konolige, and W. Burgard, “g2o: A general framework for graph optimization,” in *IEEE Intl. Conf. on Robotics and Automation (ICRA)*, 2011.
 - [37] D. Galvez-Lpez and J. D. Tardós, “Bags of binary words for fast place recognition in image sequences,” *IEEE Trans. on Robotics*, vol. 28, no. 5, pp. 1188–1197, 2012.
 - [38] J. Long, E. Shelhamer, and T. Darrell, “Fully convolutional networks for semantic segmentation,” in *IEEE Conf. on Computer Vision and Pattern Recognition (CVPR)*, 2015.
 - [39] I. Hubara, M. Courbariaux, D. Soudry, R. El-Yaniv, and Y. Bengio, “Binarized neural networks: Training neural networks with weights and activations constrained to +1 or -1,” *arXiv preprint arXiv:1602.02830*, 2016.
 - [40] K. Lin, J. Lu, C.-S. Chen, and J. Zhou, “Learning compact binary descriptors with unsupervised deep neural networks,” in *IEEE Conf. on Computer Vision and Pattern Recognition (CVPR)*, 2016.
 - [41] D. P. Kingma and J. Ba, “Adam: A method for stochastic optimization,” *arXiv:1412.6980*, 2014.
 - [42] E. Rublee, V. Rabaud, K. Konolige, and G. Bradski, “Orb: An efficient alternative to sift or surf,” in *Intl. Conf. on Computer Vision*, 2011.
 - [43] J. Xiao, A. Owens, and A. Torralba, “Sun3d: A database of big spaces reconstructed using sfm and object labels,” in *IEEE Intl. Conf. on Computer Vision (ICCV)*, 2013.